UC Irvine
UC Irvine Previously Published Works

Title

Contribution to the glaciology of northern Greenland from satellite radar interferometry

Permalink

https://escholarship.org/uc/item/0mb694v3

Journal

Journal of Geophysical Research, 106(D24)

ISSN

0148-0227

Authors

Rignot, Eric
Gogineni, Sivaprasad
Joughin, Ian
et al.

Publication Date

2001-12-27

DOI

10.1029/2001jd900071

Peer reviewed

Contribution to the glaciology of northern Greenland from satellite radar interferometry

Eric Rignot[1], Sivaprasad Gogineni[2], Ian Joughin[1], and William Krabill[3]

Abstract. Interferometric synthetic aperture radar (InSAR) data from the ERS-1 and ERS-2 satellites are used to measure the surface velocity, topography, and grounding line position of the major outlet glaciers in the northern sector of the Greenland ice sheet. The mass output of the glaciers at and above the grounding line is determined and compared with the mass input. We find that the grounding line output is approximately in balance with the input, except for the three largest glaciers for which the mass loss is 4 ± 3 km^3 ice $year^{-1}$ or $11\pm8\%$ of the mass input. Along the coast we detect a systematic retreat of the grounding lines between 1992 and 1996 with InSAR, which implies that the outlet glaciers are thinning. The inferred coastal thinning is too large to be explained by a few warm summers. Glacier thinning must be of dynamic origin, that is, caused by spatial and temporal changes in ice velocity. Iceberg production from the glaciers is uncharacteristically low. It accounts for only 8% of the ice discharge to the ocean. About 55% of the ice is lost through basal melting (5-8 m ice $year^{-1}$ on average) from the underside of the floating glacier tongues that are in contact with warm ocean waters. Mass losses are highest in the first 10 km of floating ice, where ice reaches the greatest depths and basal melting is 3 times larger than on average. Only a small increase in basal melting would suffice to disintegrate the floating glacier tongues.

1. Introduction

Early in this century, the first observations of northern Greenland glaciers were made using watches, sextant, sketch maps, and photography [*Koch*, 1928]. These observations revealed the presence of large sectors of floating ice, consolidated by the presence of nearly permanent fjord ice. Aerial photography and field studies from the 1950s showed that the glacier fronts were slowly retreating and thinning, especially in the case of tidewater glaciers [*Davies and Krinsley*, 1962]. Little information was available, however, on the rates of glacier thinning.

More recently, *Higgins* [1988, 1991] reported estimates of ice-front velocity and calf-ice production for northern Greenland. *Reeh* [1985] found that ice produced by calving was low compared with that estimated for an ice sheet in mass balance. This suggests that large uncertainties remain in the determination of the mass budget of the northern sector of the ice sheet, which represents 25% of the ice-covered area in Greenland.

Here we present a study of northern Greenland glaciers conducted using spaceborne interferometric synthetic aperture radar (InSAR) data collected between 1992 and 1996 by the European Space Agency's Earth Remote Sensing Satellites ERS-1 and ERS-2. The InSAR data were used to map the detailed ice sheet topography and vector flow [*Joughin et al.*, 1998; *Mohr et al.*, 1998] and to detect the tidally induced vertical motion of floating ice [*Rignot*, 1996] over large sectors (several hundred

kilometers). The InSAR results were combined with airborne topographic mapping (ATM) surface elevation data [*Krabill et al.*, 1999], ice-sounding radar data (ISR) [*Chuah et al.*, 1996], a new digital elevation model (DEM) of Greenland [*Ekholm*, 1996; *Bamber et al.*, 2001], and a new map of snow accumulation [*Bales et al.*, 2001]. This allowed us to obtain a more precise estimate of the mass balance of the northern sector of the Greenland ice sheet and to detect coastal thinning trends of the glaciers via the monitoring of their grounding line positions [*Rignot*, 1998a]. The paper summarizes our study and includes new ISR and ATM data collected in 1999, the analysis of additional glaciers, the detection of grounding line migration on all floating ice tongues, and vector maps of ice velocity that were not included in earlier work [*Rignot*, 1996; *Rignot et al.*, 1997a, 1997b, 2000]. We conclude on the probable state of mass balance of the northern sector of the Greenland ice sheet and on the implications of the InSAR results.

2. Study Area

Plate 1 shows a composite SAR image mosaic of the outlet glaciers considered in this study. Because our primary goal is to determine the mass balance of the northern sector of the ice sheet as a whole, we only studied the ice discharge from the largest outlet glaciers. Glaciers draining from local ice caps in Ingelfield, Nyboe, Peary, and Kronprins Christian Land and alpine glaciers draining from Nansen and Peary Land [*Weidick*, 1995] were not included. The study area is about 500,000 km^2 in size. It extends from Harald Moltke Glacier (76.5°N, 68°W) near Thule Air Base to Storstrømmen Gletscher (76.5°N, 23°W) in the east. Most outlet glaciers in that sector develop a floating glacier tongue. Few floating glacier tongues exist on the east coast south of Storstrømmen.

3. Methods

3.1. Interferometry Products

The theory of producing SAR interferograms of glaciated terrain has been described elsewhere [*Rignot et al.*, 1995;

[1]Jet Propulsion Laboratory, California Institute of Technology, Pasadena, California.

[2]Radar Systems and Remote Sensing Laboratory, University of Kansas, Lawrence, Kansas.

[3]Laboratory for Hydrospheric Processes, NASA Goddard Space Flight Center Wallops Facility, Wallops Island, Virginia.

Joughin et al., 1995; *Rignot,* 1996; *Joughin et al.,* 1996, 1998, 1999; *Mohr et al.,* 1998] and will not be repeated here. We will only summarize the salient features of our methodology.

The first InSAR observations of northern Greenland were collected in the winter of 1992 by ERS-1, then collected on a 3-day exact-repeat orbit cycle. A larger volume of data was acquired in the winter of 1995-1996 by ERS-1 and ERS-2 flying in tandem mode, i.e. ERS-2 following ERS-1 along the same orbit with a 1-day time difference. Almost no tandem data were acquired after 1996.

Double-difference SAR interferograms were used to generate topographic maps of the ice sheet with a vertical precision no better than ±20 m. These maps helped correct single-difference SAR interferograms for the effect of topography to estimate ice velocity. On floating glacier ice, satellite radar altimetry provides better topographic maps, because InSAR is contaminated by oceanic tides. For this reason we used the Greenland DEM to correct single-difference SAR interferograms for topography on floating ice and also to infer ice shelf thickness from ice shelf surface elevation. *Bamber et al.* [2001] derived their DEM by combining radar altimetry with GPS surveys, ATM, and aerial photography.

We combined single-difference SAR interferograms collected along ascending and descending tracks to produce vector maps of ice motion, except where no ascending tracks were collected (from Harald Moltke to Humboldt Gletscher). We assumed that ice flows parallel to the ice sheet surface, which is a reasonable approximation for polar glaciers. On floating ice, tidal motion was removed using the method described by *Rignot et al.* [2000], which employs tidal predictions from the FES95.2 tidal model [*Le Provost et al.,* 1998] combined with a quadruple-difference SAR interferogram. Comparisons of InSAR-derived motion vectors with GPS data in various areas of grounded ice [*Rignot et al.,* 1995; *Mohr et al.,* 1998; *Joughin et al.,* 1999] suggest that, in most favorable conditions, ice velocity is measured with a precision of 2-5 m yr^{-1}. An example vector map of ice velocity is shown in Plate 2.

Rignot [1998a] showed that grounding line positions can be mapped with InSAR with a horizontal precision of 20-50 m, which is 1-2 orders of magnitude better than in prior studies [*Rignot,* 1998b]. Grounding line positions, however, migrate back and forth with ocean tide over a rough bed. This limits the precision of mean-sea-level grounding line mapping to 100-200 m (assuming ±1-m oceanic tide and 1% thickness slope), unless multiple interferograms are analyzed. Using this approach, we detected grounding line migration between 1992 and 1996 and converted the results into thinning rates using surface slope measured by ATM and thickness slope measured by ISR.

3.2. Ice thickness

We used both measured and estimated ice thickness to compute the ice flux. The measured thicknesses were used primarily to compute mass flux using a transverse ISR profile upstream of the grounding line. These data were collected with a 150-MHz coherent radar, operated on an aircraft equipped with GPS receivers. The uncertainty in ice thickness is 10 m [*Rignot et al.,* 1997b]. Only a few ice thickness measurements were made across the glacier at grounding lines because of the inherent difficulties of flying the aircraft across deep fjords and processing radar echoes in the proximity of steep rock and ice faces. We estimated the grounding line thickness from ice shelf elevation from DEM or ATM data, assuming hydrostatic equilibrium of the ice. We used a multiplicative factor of 9.115 to convert grounding line elevation to ice thickness.

In Table 1 we compare the results with ISR at the point of crossing with the grounding line. The average error is 8±13% of the actual thickness. Large deviations (30%) exist on a few glaciers (Hagen Brae and Storstrømmen), which are not in equilibrium because they are surge-type glaciers. An ad hoc correction (i.e., an absolute bias and a new multiplicative factor) is applied on the DEM data to reduce the uncertainty in derived thickness. The precision of the corrected thickness is estimated to be 20-50 m (last column of Table 1 and Fig. 1).

3.3. Ice Fluxes

We calculated the ice flux both at the grounding line and upstream of the grounding line when transverse ISR data were available. We computed the flux at two locations to increase confidence in the estimates of grounding line discharge and to estimate the glacier mass balance at higher elevation, where ice dynamics and ablation effects are presumably less significant.

We calculated ice front fluxes for a few glaciers and also compiled published data on a few others. The difference in ice flux between the grounding line and the ice front, divided by the ice shelf area in between, yields an estimate of the glacier net balance on floating ice. Comparing the result with accumulation minus surface ablation, we deduced an average basal melting rate under steady state conditions. Similarly, we calculated the average basal melting rate for the first 10 km of floating ice, where basal melting is higher. If the floating ice tongues are not in steady state and are for instance thinning 1-2 m yr^{-1}, conservation of mass dictates that basal melting should exceed the calculated steady state rates by the same amount.

For a typical grounding line thickness of 600 m with an uncertainty of 30 m and a grounding line velocity of 1000 m yr^{-1} with an uncertainty of 4 m yr^{-1}, the error in mass flux is 5%. With a 10% uncertainty for surface melt on ice shelves, the error in steady state basal melting is 12%.

3.4. Glacier Topography

The ATM laser instrument on the aircraft flying at 500 m above the ice surface scans over a 50-m swath, centered at about the nadir point on the ice surface. ATM surface elevations have a height measurement accuracy of 10 cm [*Krabill et al.,* 1999]. We used ATM data to identify hydrostatic equilibrium of the ice (Table 1 and Figures 1 and 2) in the proximity of the InSAR-derived grounding lines. A few outlet glaciers were also surveyed repeatedly to measure elevation changes between 1994 and 1999.

We utilized the Greenland DEM to delineate individual drainage basins from the end points of the flux gates, following the line of steepest slope. We matched the end points of the grounding line and ISR flux gates along flow lines to conserve mass between flux gates. Radar altimeters do not measure surface slope well near the ice sheet margin, i.e., right above the grounding line. Because of this we used clearly defined flow line features visible in the SAR imagery to initiate the drainage boundaries at low elevation. This procedure was extended to higher elevation until the line of steepest slope derived from the DEM is aligned with flow line features in the SAR imagery.

3.5. Mass Accumulation

Annual precipitation is low in northern Greenland, ~100-300 mm water equivalent (w.e.) in the humid coastal areas and < 100 mm in the interior [*Weidick,* 1995]). The 1993-1994 German expedition in east Greenland [*Friedman et al.,* 1995] revealed that *Ohmura and Reeh* [1991] overestimated accumulation in the north. This was confirmed with recent ice cores [*Bales et al.,*
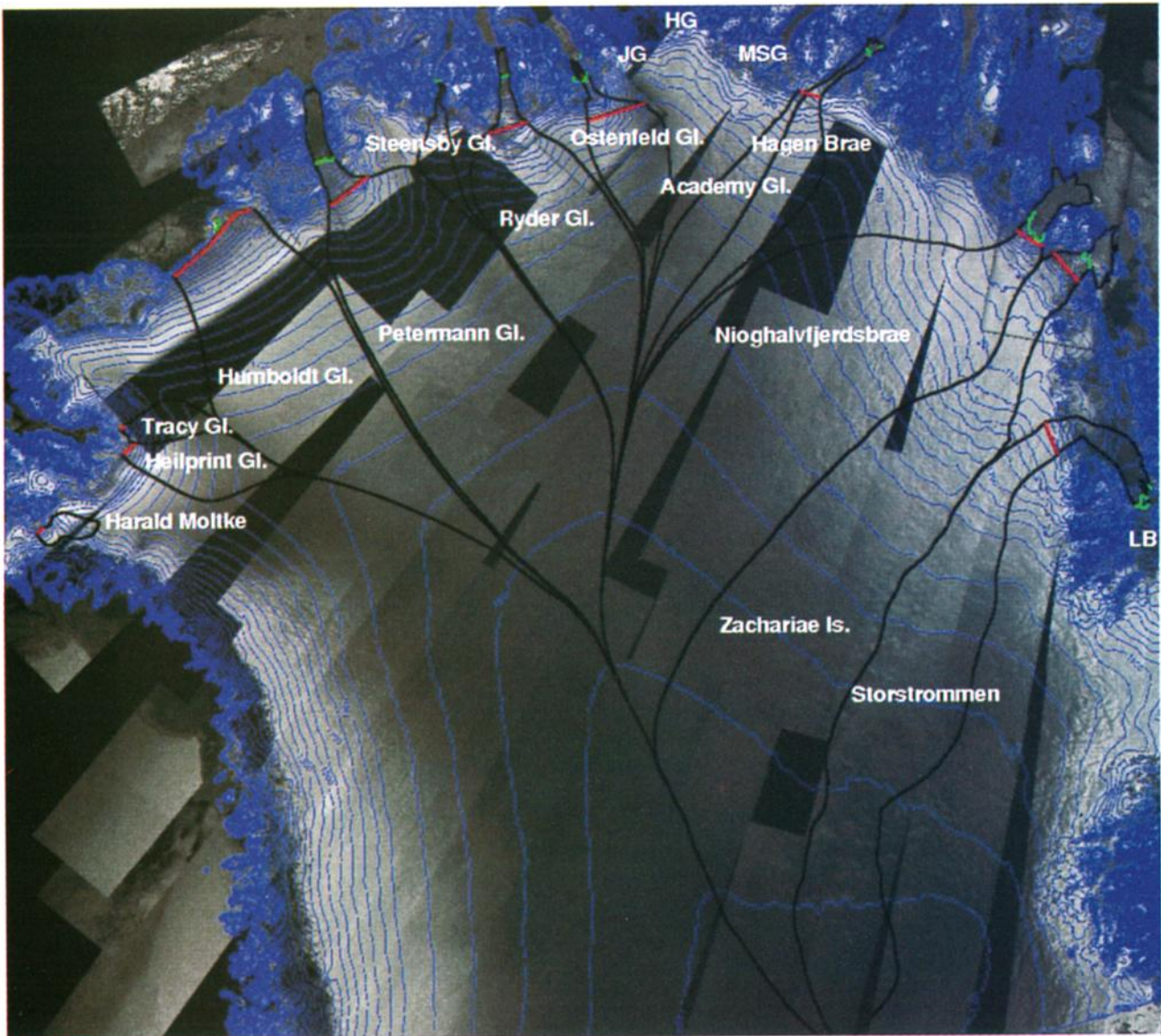
Plate 1. ERS synthetic aperture radar (SAR) mosaic of northern Greenland glaciers on a polar stereographic grid (courtesy National Snow and Ice Data Center, complemented by data from this project). Ice-sounding radar (ISR) lines used to calculate fluxes are shown in red; grounding lines from 1996 are green; drainage basins are black; digital elevation model (DEM) contour lines (every 100 m from 100 m to 2000 m and every 200 m thereafter) are blue. Abbreviations are as follows: JG, Jungersen Gletscher; HG, Henson Gletscher; MSG, Marie Sophie Gletscher; and LB, L. Bistrup Brae. ERS imagery ©ESA 1996.
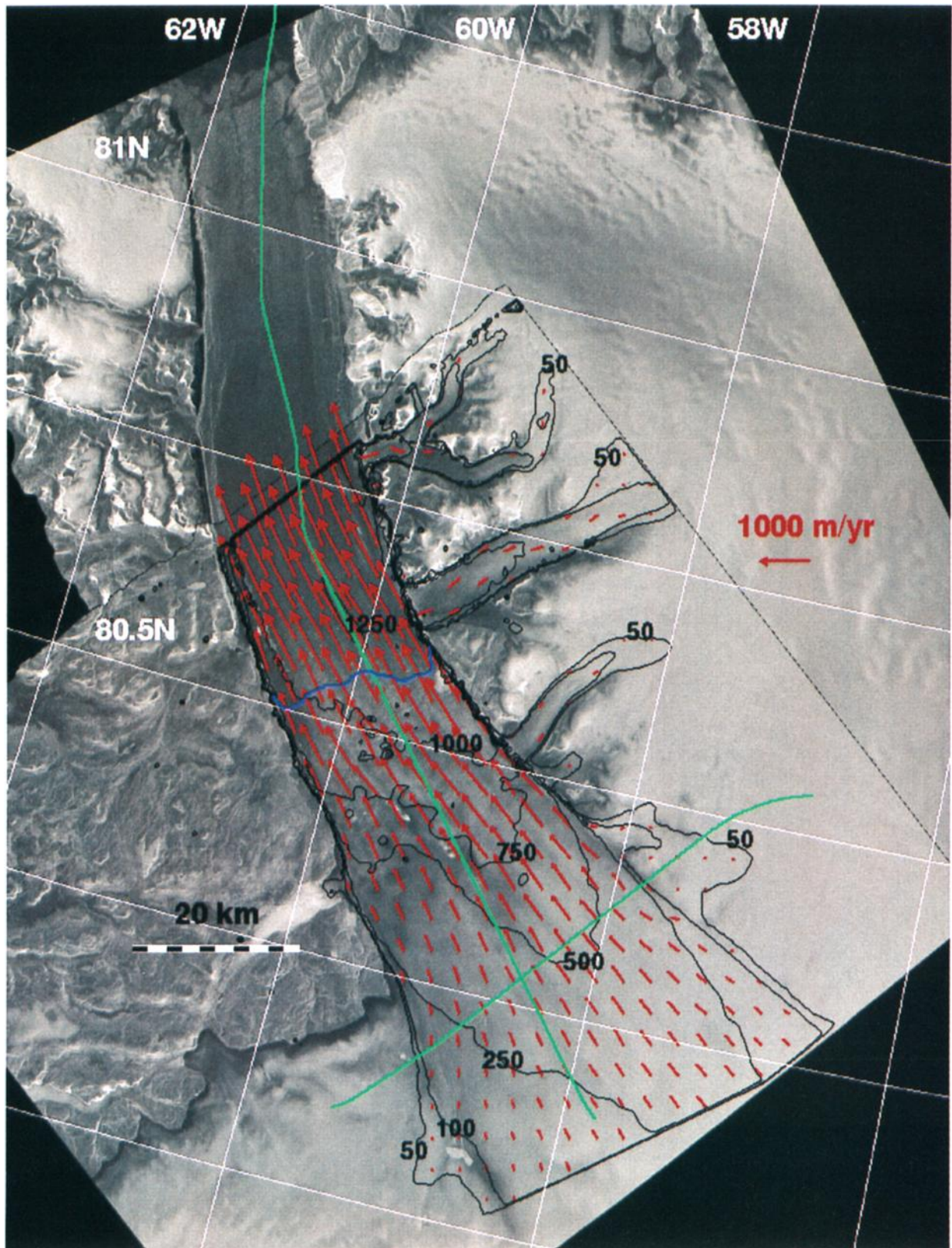
Plate 2. Vector velocity map of Petermann Gletscher derived from ERS InSAR ascending and descending tracks. The grounding line is shown in white for 1996 and in black for 1992. Flow vectors are red. Velocity contours are blue. ISR lines are green. Vector velocity maps for Ryder Gletscher, Nioghalvfjerdsbrae and Zachariae Isstrøm, and Storstrømmen are shown by *Joughin et al.* [1998], *Rignot et al.* [2000], and *Mohr et al.* [1998], respectively.

Table 1. Glacier Thickness at the Grounding Line[a].

Glacier	Year	H_{ISR}	H_{DEM}	$h_{DEM\text{-}ATM}$	H_{ISR}/H_{ATM}	$\underline{H}_{DEM}$
Petermann	1995	544±2	654±18	+5±1	9.7±1.1	554
Petermann	1999	550±3	649±16	+5±2	9.5±1.3	549
Ryder	1997	406±6	480±6	+16±1	10.8±0.5	400
Hagen Brae[b]	1999	173±25	638±48	+48±2	8.8±1.0	193
Nioghalvfjerdsbrae S	1995	639±2	619±3	+0±0	10.3±1.0	683
Nioghalvfjerdsbrae C	1999	744±1	614±13	-12±0	10.3±0.7	678
Zachariae Isstrøm N	1999	564±2	648±28	+21±1	10.9±1.3	584
Zachariae Isstrøm S	1999	527±35	598±38	+14±1	10.9±1.3	525
Storstrømmen	1997	422±3	441±2	+10±1	11.1±0.4	441
Storstrømmen	1999	507±2	1143±3	+13±0	11.0±0.4	NA
L. Bistrup Brae	1997	391±19	361±22	-19±10	11.1±0.4	NA
L. Bistrup Brae	1999	452±10	773±16	+16±1	11.0±0.4	NA

[a] Data presented are glacier name, year the ice sounding radar (ISR) data was collected, thickness measured with ISR (H_{ISR}), thickness calculated from a digital elevation model (DEM) of Greenland (H_{DEM}, h_{DEM} x 9.115), difference in ice shelf elevation between the DEM and airborne topographic mapper (ATM) data ($h_{DEM\text{-}ATM}$), ratio of the ISR thickness by the ATM thickness (H_{ISR}/H_{ATM}), and thickness calculated from the DEM after correction ($\underline{H}_{DEM}$). In glacier name, S means south, C, center, and N, north sector of the grounding line. Glacier thickness is given in meters.
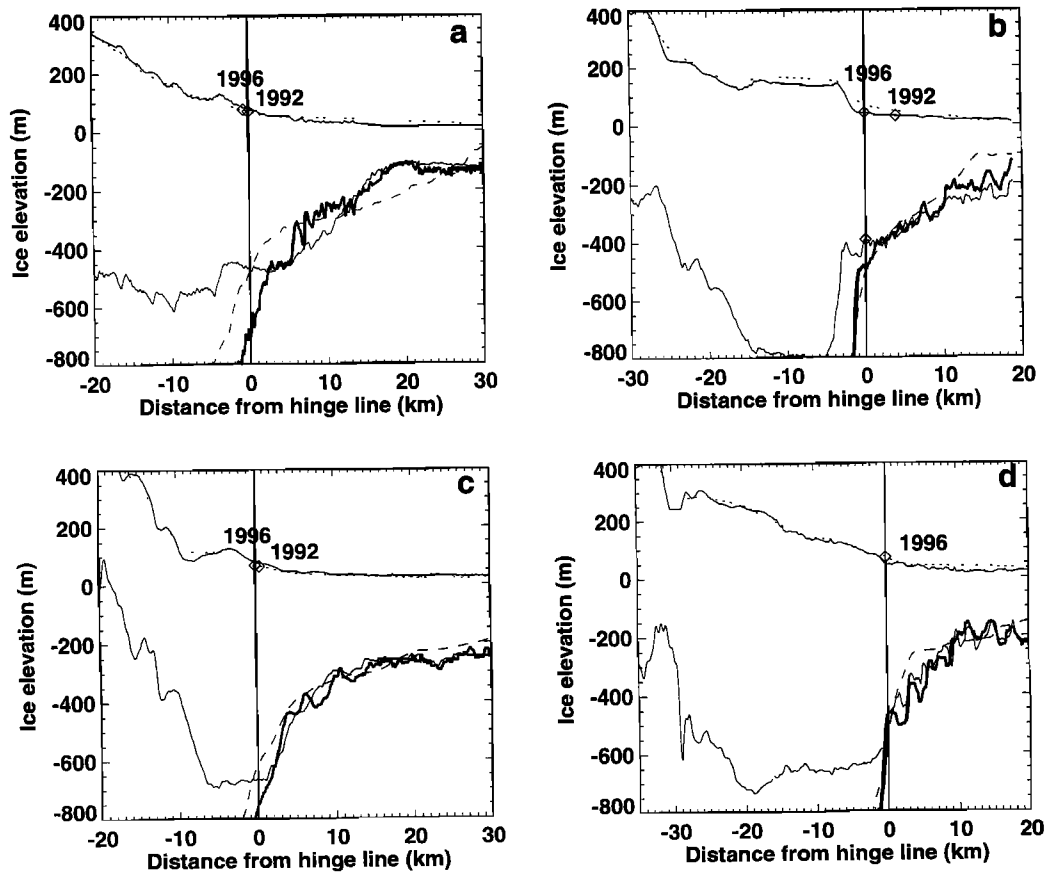[b] Values are given for ice shelf with elevation anomaly.

Figure 1. Along-flow surface and bed elevations of (a) Petermann Gletscher on May 10, 1999; (b) Ryder Gletscher on May 23, 1999; (c) Nioghalvfjerdsbrae on May 19, 1999; and (d) Zachariae Isstrøm on May 19, 1999. Surface elevations are from airborne topographic mapping (ATM) (solid line) and DEM (dotted line). Thicknesses are from ISR (thin solid line), deduced from hydrostatic equilibrium of the ice using ATM (bold line) and corrected-DEM elevations (dashed line). Grounding line positions are marked with a diamond. The point of first hydrostatic equilibrium of the ice is at the crossing of the ISR thickness with the ATM-derived thickness.

Figure 2. Grounding line migration measured with interferometric SAR (InSAR) between 1992 and 1996 on (a) Humboldt Gletscher, (b) Petermann Gletscher, (c) Steensby Gletscher, (d) Ryder Gletscher, (e) C. H. Ostenfeld Gletscher, (f) Hagen Brae, (g) Nioghalvfjerdsbrae; (h) Zachariae Isstrøm (no 1992 InSAR), and (i) Storstrømmen and L. Bistrup Brae. The location of the grounding line is shown in black for 1992 and in white for 1996, and marked with a pointing arrow. ISR lines are shown in white for 1995 and in solid black for 1999. Intercepts between grounding lines and ISR are marked as diamonds. Bold lines in Figures 2b, 2c, 2d, and 2f-2i denote portions of the ISR track for which ice is in hydrostatic equilibrium, shown in white for 1995 and in black for 1999. Figure 2b includes a 1999 transverse ISR line used to estimate the grounding line ice flux; no ATM elevation was available for that flight because of cloud cover. All plots are overlaid on the radar brightness of the scene from ERS. ERS imagery ©ESA 1996.

Table 2. Equilibrium Line Altitude[a].

Glacier	ELA P	ELA ERS	ELA M	DDF
Harald Molke Brae	900[b]	700	720	9.8/3.0
Heilprin/Leidy/Marie	900[b]	900	803	9.8/3.0
Tracy	900[b]	900	948	9.8/3.0
Humboldt	600-800[b]	700	733	6.9/2.1
Petermann	800-900[c, d]	800	747	9.8/3.0
Ryder/Steensby	800[c]	800	768	9.8/3.0
C.H. Ostenfeld	NA	800	710	9.8/3.0
Academy	900-1000[c]	800	954	9.8/3.0
Hagen Brae	NA	800	954	9.8/3.0
Nioghalvfjerdsbrae	NA	800	937	4.9/1.5
Zachariae Isstrøm	NA	800	1002	4.9/1.5
Storstrømmen	1100[e]	1100	1170	9.8/3.0
L. Bistrup Brae	NA	1000	1086	9.8/3.0

[a] Data presented are glacier name, equilibrium line altitude (ELA) published in the literature (ELA P), estimated from ERS (ELA ERS), estimated from a degree day model (ELA M), and degree day factor for ice / snow (mm °C^{-1} d^{-1}), respectively, used in the degree day model (DDF).
[b] Source is *Nobles* [1960].
[c] Source is *Weidick* [1995].
[d] Source is *Koch* [1928].
[e] Source is *Bøggild et al.* [1994].

2001]. In the case of the combined drainage basin from the six largest glaciers the new accumulation numbers are 11% lower than those employed by *Rignot* et al. [1997a], which were based on the work of *Ohmura and Reeh* [1991]. *Rignot et al.* [2000] employed a preliminary version of the new accumulation map that yields a total snow accumulation 4% larger than in this study. We estimate that an accumulation accuracy of 5% is a reasonable assumption for the entire domain of study, but the uncertainty may be > 10% over small areas.

3.6. Mass Ablation

Few studies of mass ablation have been conducted in the north (at "Red Rock" near Thule Air Base [*Nobles*, 1960; *Goldthwait*, 1971], in Christian Erichsen Iskappe in Peary Land (77°N, 25° W) [*Høy*, 1970], on Britannia Glacier, in Dronne Louise Land (77°N, 24.5°W) [*Lister*, 1958], in Kronprins Christian Land (KPCL) (80°N, 24 °W) [*Konzelmann and Braithwaite*, 1995], in Hans Tausen Iskappe (HTI) (83°N, 36°W) [*Braithwaite et al.*,

1998], and on Storstrømmen (77°N, 23°W) [*Bøggild et al.*, 1994]). The results suggest large interglacier variability in radiation budget: The degree day factor for ice at KPCL is 9.8±0.9 versus 5.9±0.6 at HTI.

In a prior assessment of ice sheet mass balance we used *Reeh*'s [1991] degree day model with a degree day factor of 9.8 mm deg^{-1} day^{-1} w.e. for ice [*Braithwaite*, 1992] and 3.0 mm deg^{-1} day^{-1} w.e. for snow. These values are higher than those derived for western Greenland [*Braithwaite*, 1995, 1996] because cloud cover is reduced in northern Greenland [*van der Wal*, 1996].

In Table 2 we adjusted the degree day factor for each glacier to reproduce either a published value of the glacier equilibrium line altitude (ELA) or its presumed location on ERS imagery. This is based on a method discussed by *Joughin et al.* [1999] and *Rignot et al.* [2000]. The ELA depends on the degree day factor for snow, which we assume to be equal to 40% the degree day factor for ice, following *Braithwaite* [1996]. Changing the degree day factor for snow from 0.3 (high value) to 0.18 (low value) decreases the ELA by 200 m. The ELAs in Table 2 are not

Table 3. Mass Balance at the ISR Flux Gate[a].

Glacier	V	H	IF	AA	AC	AB	BF	MB
Heilprin	548	1,036	2.19	7,083	1.71	0.05	1.66	- 0.53
Tracy	516	1,213	1.43	2,969	0.68	0.13	0.55	- 0.88
Humboldt	350	500	6.25	44,214	8.56	2.42	6.14	- 0.11
Petermann	553	1,050	12.82	68,573	12.41	0.19	12.21	- 0.61
Ryder	270	1,100	3.88	27,836	4.75	0.06	4.69	+0.81
Ostenfeld	153	800	2.32	8,573	1.50	0.00	1.50	- 0.82
Academy	150	1,200	0.69	9,561	1.39	0.01	1.38	+0.69
Hagen Brae	130	1,100	1.03	10,057	1.52	0.01	1.50	+0.47
Nioghalvfjerdsbrae	1,250	700	14.27	96,093	12.54	1.12	11.41	- 2.86
Zachariae Isstrøm	500	800	11.65	92,095	13.12	1.51	11.61	- 0.04
Storstrømmen	230	1,040	5.80	51,465	7.80	0.03	7.77	+1.97
Total			62.3	418,519	66.0	5.5	60.4	- 1.9

[a] Data presented are as follows: V, center velocity (m yr^{-1}); H, center thickness (m); IF, ice flux at the ISR flux gate (km^3 ice yr^{-1}); AA = drainage area above the ISR flux gate (km^2); AC, AB, and BF accumulation, ablation, and balance flux (BF = AC − AB) at the ISR flux gate (km^3 ice yr^{-1})., and MB, mass balance (MB = BF − IF) at the ISR flux gate (m ice yr^{-1}).

Table 4. Mass Balance at the Grounding Line.[a]

Glacier	V	H	GF	CF	AA	AC	AB	BF	MB
Petermann	1,160	630	11.67	0.59[b]	69,706	12.71	1.82	10.89	- 0.78
Steensby	270	460	0.51	0.26	3,040	0.73	0.16	0.57	+0.06
Ryder	540	620	2.29	0.66[b]	28,707	4.96	0.91	4.04	+1.75
Ostenfeld	810	600	2.27	0.54[b]	9,481	1.67	0.34	1.33	- 0.94
Hagen Brae	61	200	0.07	0.36[b]	10,629	1.61	0.57	1.04	+0.97
Nioghalvfjerdsbrae	1,300	650	14.19	0.90	96,309	12.56	1.42	11.14	- 3.05
Zachariae Isstrøm	1,100	550	10.81	1.10	92,680	13.19	2.34	10.85	+0.04
Storstrømmen	15	530	0.03	0.90[c]	54,605	8.37	7.09	1.28	+1.25
Total			41.8	5.37	365,157	55.7	5.5	60.4	- 0.7

[a] Data presented are as follows: V, center velocity (m yr^{-1}); H, center thickness (m); GF, ice flux at the grounding line (GL) (km^3 ice yr^{-1}); CF, calving flux or ice flux at the ice front (km^3 ice yr^{-1}); AA = drainage area above the GL flux gate (km^2); AC, AB, and BF accumulation, ablation, and balance flux (BF = AC − AB) at the GL flux gate (km^3 ice yr^{-1})., and MB, mass balance (MB = BF − GF) at the GL flux gate (m ice yr^{-1}).
[b] Source is *Higgins* [1991].
[c] Source is *Reeh et al.* [1994].

known with a precision better than 100 m vertical, or 10 km horizontal. This level of precision is sufficient to reduce the uncertainty in surface melt to an acceptable level.

Most glaciers fit the higher degree day factor, except for three. In the case of Nioghalvfjerdsbrae we calculate a net ablation of 2.8 km^3 ice yr^{-1} for the floating tongue using the lower degree day factor, compared to 3.0 km^3 ice yr^{-1} estimated by *Reeh et al.* [1999] using unpublished in situ measurements. Our new estimates of surface ablation should therefore have an uncertainty of 10% for the entire study area. Larger errors (20-30%) are not to be excluded on small areas. While this uncertainty is large, it has a limited impact on the mass balance estimates. In Table 3, ablation accounts for 10% of the mass budget, hence yielding only a 1% uncertainty in mass balance. In Table 4, ablation is 28% of the mass budget and contributes a 3% uncertainty. By measuring ice fluxes at and upstream of the grounding line, we avoid dealing with the bulk of surface ablation that prevails at lower elevation.

Overall, the balance flux for each glacier is not known with a precision better than 10%, but the balance flux for the entire sector of study should be reliable at the 6% level (5% for accumulation and 3% for ablation). The mass balance estimates should therefore be accurate at the 8% level.

4. Results of the Glacier Survey

Here we describe the mass balance, grounding line migration and basal melting results obtained from each glacier, starting from the west and moving toward the east. For some glaciers, no results are included in Tables 3-6, for reasons described below in sections 4.1, 4.6, 4.7 and 4.9, but we discuss new information relevant to their state of mass balance.

4.1. Harald Moltke, Heilprin, and Tracy Glaciers

The 1996 ERS data show no floating section for these three glaciers. This is consistent with [*Koch*, 1928] in the case of Harald Moltke, but it is contrary to the *Davies and Krinsley* [1962] reports on Heilprin and Tracy Glaciers. These two glaciers have probably thinned and retreated considerably since 1957.

Harald Moltke is a surge-type glacier [*Mock*, 1966]. It drains from local ice domes, not from the inland ice as presumed in prior studies. Hence it is not included in Tables 3-6. At the ice front it is 5 km wide and 400 m thick and flows at 90 m yr^{-1}. This yields a mass flux 25% lower than the balance flux at that location. At the ISR flux gate located 30 km upstream, ice discharge is 26% larger than the balance flux. This balance pattern suggests that ice accumulates between the front and the ISR gate, perhaps in prelude to the next surge.

Kollmeyer [1980] documented a large retreat for Heilprin and Tracy Glaciers, with Tracy Gletscher retreating the most (7 km between 1892 and 1959). The ice discharge in Table 3 is lower than that estimated by *Weidick* [1995], perhaps because the glaciers slowed down in recent times. It is significantly larger (33%) than the balance discharge, however, which suggests significant thinning in this sector of the ice sheet.

Table 5. Steady State Basal Melt Rates of the Floating Glacier Tongues in Northern Greenland.[a]

Glacier	Entire ice shelf				Ice shelf within 10km of GL			
	NB	ISA	ABA	BM	NB$_{10}$	ABA$_{10}$	ISA$_{10}$	BM$_{10}$
Petermann	-8.4	1,304	-2.2	6	12.71	-2.2	263	22
Steensby	-7.1	36	-1.2	6	0.73	NA	NA	NA
Ryder	-10.0	245	-1.6	8	4.96	-1.5	101	25
Ostenfeld	-12.6	137	-1.1	11	1.67	-1.1	49	26
Nioghalvfjerdsbrae	-6.5	1,874	-1.3	5	12.56	-1.3	318	26
Zachariae Isstrøm	-10.0	1,065	-1.5	8	13.19	-1.5	170	25

[a] Data presented are as follows for entire ice shelf (i.e., between grounding line (GL) and ice front): NB, ice shelf net mass balance (NB = (CF - GF) / ISA in m ice yr^{-1}, with CF and GF listed in Table 4); ISA, ice shelf area (km^2); ABA, ablation minus accumulation (m ice yr^{-1}); and BM, average basal melt rate (BM = (NB - ABA) in m ice yr^{-1}). For ice shelf area between the grounding line and a flux gate located 10 km downstream, the notation is as follows: NB$_{10}$, ice shelf net mass balance; ISA$_{10}$, ice shelf area; ABA$_{10}$, ablation plus accumulation; and BM$_{10}$, basal melt rate. Positive values of BM or BM$_{10}$ indicate melt.

Table 6. Grounding Line Migration.[a]

Glacier	1992	1996	δx	α	β	δh	δs
Humboldt	79.683/-64.43	79.682/-64.39	-780	-1.1	+1.0	-1.7	-1.0±0.5
Petermann	80.562/-59.89	80.559/-59.88	-450	-1.0	-1.0	-1.3	NA
Steensby	81.470/-54.41	81.469/-54.44	+105	-0.8	-0.7	+0.2	NA
Ryder	81.619/-50.48	81.581/-50.44	-4,200	-0.5	+1.0	-4.0	-1.0±0.6
Ostenfeld	81.600/-45.29	81.595/-45.27	-500	-1.0	NA	-1.2	NA
Hagen Brae	81.439/-27.45	81.437/-27.47	-390	-2.2	+5.6	-1.6	-2.5±1.5
Nioghalvfjerdsbrae E	79.274/-22.37	79.270/-22.38	-450	-0.9	-3.2	-1.5	NA
Nioghalvfjerdsbrae C	79.361/-22.46	79.357/-22.49	-650	-1.2	+0.7	-1.7	NA
Zachariae Isstrøm	NA	78.910/-20.61	NA	NA	NA	NA	-0.3±0.3
Storstrømmen S	76.730/-22.72	76.724/-22.72	+658	-0.4	+0.4	+0.6	-2±0.5
Storstrømmen N	76.760/-22.61	76.773/-22.60	-1,395	-0.1	+0.6	-0.0	NA
L. Bistrup Brae W	76.679/-22.74	76.651/-22.82	+3,708	+0.5	-0.5	+4.0	+0.5±1
L. Bistrup Brae E	76.666/-22.68	76.639/-22.69	+3,092	-1.0	+0.7	+7.0	NA

[a] Data presented are glacier name, latitude/longitude (deg) of crossing of the 1992 grounding line (GL) with the ice sounding radar (ISR) data line, latitude/longitude of crossing of the 1996 GL with ISR, horizontal migration of the GL between 1992 and 1996 measured with INSAR in meters (δx, positive value means GL advance), glacier surface slope in percent counted positive upwards (α),bed slope in percent counted positive upwards (β), change in ice thickness calculated from the rate of GL migration in m yr^{-1} (δh), and thickness change in m yr^{-1} measured with ATM between 1994 and 1999 (δs).
[b] Source is *Rignot* [1998a].
[c] Source is *Rignot et al.* [2000].

4.2. Humboldt Gletscher

Humboldt Glacier is 110 km wide at the calving front, with a low rate of movement. ERS data confirm earlier observations [*Kollmeyer*, 1980] that most of the glacier front is grounded, except for a few places that float at high tide in the southern sector. The northern sector flows faster and develops a permanent floating section (Figure 2a). The glacier is close to a state of mass balance at the ISR flux gate (Table 3). A division of the glacier drainage into a northern and southern sectors, however, reveals that the northern sector exhibits a more negative mass balance than the southern sector (not shown in Table 3). This result is consistent with ATM measurements which show more pronounced thinning in the north than in the south [*Abdalati et al.*, this issue].

The grounding line retreated 1 km between 1992 and 1996, which implies a thinning of 1.7 m ice yr^{-1} (Table 6). The ATM measurements collected 20 km farther north revealed a 1±0.5 m yr^{-1} thinning rate, which is consistent with our estimate. Humboldt Gletscher is therefore thinning in the north, where ice flows fast, and is closer to equilibrium in the south, where ice moves slowly.

4.3. Petermann Gletscher

Petermann Gletscher is a fast moving glacier that develops a 20-km-wide by 70-km-long floating tongue. We improved our earlier estimates of its grounding line flux by using a vector map of ice velocity (Plate 2) and a corrected DEM (Table 1). The new estimate is in agreement with that computed using a transverse ISR profile collected in May 1999, a few kilometers upstream of the grounding line (Figure 2b). The glacier mass balance is negative, -7% of the balance flux at the grounding line (Table 4) and is -5% at the ISR flux gate (Table 3).

The grounding line retreated 450±100 m between 1992 and 1996 at the crossing point with the 1995 ISR data, which implies a thinning rate of 1.3 m ice yr^{-1} (Table 6). The average retreat rate across the glacier width is 270 m, which implies 0.8 m ice yr^{-1} thinning.

The line of first hydrostatic equilibrium of the ice is located 1.5 km downstream of the InSAR-derived grounding line. Similar offsets are found for other glaciers. In 1999 the limit of hydrostatic equilibrium is detected south of its 1996 position

(Figure 2b), which suggests that the grounding line continued its slow retreat.

The calf-ice production from this glacier is 20 times lower than its grounding line discharge (Table 4). The net balance of the floating tongue is -8.4 m ice yr^{-1} (Table 5), of which -2.2 m ice yr^{-1} is due to surface runoff plus accumulation, and the rest is due to basal melting [*Rignot*, 1996]. Overall, 70% of the ice is lost from basal melting, 25% is lost from surface melting, and the rest is lost from calving (icebergs). This division of process differs markedly from that of glaciers located farther south, where ice discharge is evenly partitioned between surface melting and calving [*Reeh et al.*, 1999].

4.4. Newbugt Glacier and Steensby Gletscher

The 2-km-wide Newbugt Glacier flows between Hall and Nyeboe Land [*Higgins*, 1991], with minimal ice discharge. We found no floating section in 1996, whereas *Higgins* [1991] reported that the frontal 1 km was afloat. The ice velocity decreased from 35-45 m yr^{-1} in the 1970s [*Higgins*, 1991] to 19-20 m yr^{-1} in 1996. The glacier is likely in a state of retreat.

The 4.5-km-wide Steensby Gletscher has a mass budget close to zero (Table 4). Its 1996 velocity is similar to that measured by *Higgins* [1991] in the 1970s. Its grounding line advanced slightly (Figure 2c), which implies a slight thickening of the glacier (Table 6). The average basal melting rate of its floating tongue is similar to that estimated on other glaciers (Table 5).

4.5. Ryder Gletscher

The 8-km-wide Ryder Gletscher drains into Sherard Osborn Fjord. *Davies and Krinsley* [1962] reported a large retreat of the glacier prior to 1947, with further retreat by calving between 1947 and 1958. Ryder Gletscher experienced a mini surge in 1995, which more than tripled its ice velocity on October 26-27, 1995 [*Joughin et al.*, 1996]. By November 8-9, the velocity returned to normal values observed on September 21-22. Additional data subsequently revealed that the glacier velocity was still normal on October 10-11, 1995. The mini surge of 1995 therefore lasted less than 3.7 weeks.

Two successive, large, transverse ridges revealed by the ISR data (one ridge is shown in Figure 1c at -3 km, another is shown by *Joughin et al.* [1999]) obstruct the glacier flow into the fjord.

This unusual bed configuration probably plays a major role in the ponding of basal melt water upstream of the grounding line, which was suggested to be responsible for the pulsing (surge) behavior of the glacier.

If the glacier were to triple its velocity for 4 weeks every year, it would discharge 15% more ice than listed in Table 4. This would reduce its positive mass balance from 43 to 28%. The glacier would need to surge for longer time periods (12 weeks) every year to be in balance with its mass input. At the ISR flux gate the glacier balance reduces to 17% (Table 3).

The grounding line retreated 4.2 km between 1992 and 1996, which is the largest retreat in our study area (Figure 2d). The retreat implies a thinning of 4 m ice yr^{-1} (Table 6). Most likely, the glacier lost a large quantity of ice during the surge. At the location of the 1996 grounding line the ATM data indicate a 2-m thinning between 1997 and 1999. In 1999 the line of hydrostatic equilibrium migrated upstream of its 1997 position (Figure 2d), which also suggests glacier thinning. One possible way to reconcile the thickening indicated by the ice fluxes with the thinning indicated by InSAR and ATM is that the glacier drainage basin is overestimated in the DEM (see section 4.6).

4.6. C.H. Ostenfeld Gletscher and Harder and Brikkerne Glaciers

These glaciers drain into Victoria Fjord (Figure 2e). Ostenfeld Gletscher is the largest and most active glacier. Its 7-km-wide disconnected floating segment moved at 800 m yr^{-1} in 1996, as in the early 1960s, with a similar ice tongue configuration [*Higgins and Weidick*, 1988]. Brikkerne Gletscher, which flows from the northeast, is a surge-type glacier. The 1996 velocity of its three branches is lower than that recorded in 1978 but is comparable to that recorded in 1963, prior to a surge. Harder and Brikkerne Gletscher are nourished from a local ice dome, not from the inland ice, and are therefore not included in Tables 3-6.

The mass balance of Ostenfeld Gletscher is -71% at the grounding line (Table 4) and –50% at the ISR flux gate (Table 3). Its drainage basin is bound by a dome to the north and by Ryder Gletscher to the south. If the divide between Ryder and Ostenfeld Glaciers is correct, Ostenfeld Gletscher must experience massive thinning at present. Most likely, some of the flow attributed to Ostenfeld Gletscher belongs to Ryder Gletscher. The combined mass budget of both glaciers is close to balance in Table 4.

The grounding line of Ostenfeld Gletscher retreated 500±200 m between 1992 and 1996 (Figure 2e), which implies 1.2 m ice yr^{-1} thinning. This result confirms the probable state of retreat of this glacier, independent of its mass input.

4.7. Jungersen, Henson, Marie Sophie, Academy, and Hagen Glaciers

The importance of Jungersen and Henson Glaciers was exaggerated in earlier work [*Koch*, 1928]. Both glaciers exhibit floating sections, with minimal discharge. The drainage basins are not well defined in the Greenland DEM.

Marie Sophie and Academy Glaciers discharge into Independence Fjord and exhibited no floating section in 1996. Marie Sophie Gletscher reduced its ice velocity by half since the 1970s [*Higgins*, 1991], while the 8.5-km-wide Academy Gletscher maintained a velocity of 270 m yr^{-1}. The mass budget of Academy Gletscher is largely positive, which is not consistent with the state of retreat reported by *Davies and Krinsley* [1962]. The divide between Academy Gletscher and Hagen Brae, however, is uncertain since the two glaciers merge at the location of the ISR profile at about 1000 m elevation (Plate 1).

Hagen Brae is a 10-km-wide outlet glacier whose ice front is dammed by two islands. The glacier overrides a large transverse

ridge at the grounding line. The 1996 ice front velocity of 94 m yr^{-1} is considerably lower than the 510-540 m yr^{-1} reported by *Higgins* [1991], which suggests anomalously low glacier velocity in 1996. The 1996 glacier velocity decreases from the ELA to near-zero values at the ice front, similar to the velocity profile of Storstrømmen, a surge-type glacier in the northeast [*Reeh et al.*, 1994]. As a result, the glacier mass budget is largely positive at the grounding line and is closer to zero at the ISR flux gate (Tables 3 and 4). These observations suggest that Hagen Brae is a surge-type glacier, which surged in the 1970s and is now in a quiescent mode.

The grounding line of Hagen Brae retreated 400 m between 1992 and 1996 (Figure 2f), which translates into a thinning of 1.6 m yr^{-1} comparable to that measured with ATM (Table 6). Because the glacier is nearly stagnant at the grounding line, it is probably thinning at its ablation rate.

4.8. Nioghalvfjerdsbrae and Zachariae Isstrøm

This sector of northern Greenland is discussed by *Thomsen et al.* [1997], *Rignot et al.* [1997a], *Joughin et al.* [this issue], and *Reeh et al.* [1999]. A major retreat of the outlet glaciers must have taken place in the first half of the century since Zachariae Isstrøm and Nioghalvfjerdsbrae used to form coalescent ice tongues [*Weidick*, 1995]. These glaciers also serve as outlets for the northeast ice stream, an unusual flow feature in Greenland.

The mass budget of Nioghalvfjerdsbrae is negative (Tables 3 and 4), whereas the mass budget of Zachariae Isstrøm is close to zero. The divide between Nioghalvfjerdsbrae and Zachariae Isstrøm is, however, difficult to define with certainty for hundreds of kilometers upstream of the grounding lines. A more reliable indication of the mass balance of this sector is that their combined ice discharge exceeds the balance flux by 12%. They are therefore likely losing mass at present.

The grounding line of Nioghalvfjerdsbrae retreated 400-600 m at the glacier center between 1992 and 1996 (Figure 2g), which implies 1.7 m ice yr^{-1} thinning (Table 6). On the southern flank of Nioghalvfjerdsbrae, hydrostatic equilibrium migrated inland in 1999 compared to 1996 (Figure 2g), that is, the grounding line probably continued to retreat after 1996. Similarly, on Zachariae Isstrøm, for which no InSAR data exist prior to 1996, the region of hydrostatic equilibrium migrated inland between 1995 and 1999 (Figures 1 and 2h), which suggests glacier thinning.

4.9. Storstrømmen and L. Bistrup Brae

The velocity of Storstrømmen was deemed to be considerable by *Higgins* [1991] (1.8 km yr^{-1}), but the glacier was found to be stagnant in the 1990s [*Mohr et al.*, 1998]. Storstrømmen is a surge-type glacier. Its current low level of ice discharge explains its largely positive mass budget (Tables 3 and 4).

The grounding line of Storstrømmen exhibits a mixture of retreat and advance (Figure 2i). The retreating sector has a very low surface slope, which implies no thinning (Table 6). The advancing southern sector thickened slightly between 1992 and 1996. The ATM instrument measures a thinning of 2 m yr^{-1} between 1994 and 1999. Because the velocity is very low, the glacier is likely thinning at its ablation rate. Surface ablation varies strongly from year to year [*Bøggild et al.*, 1994] and was unusually high in 1997, which was a record warm year in northern Greenland (K. Steffen, personal communication 1999). The difference in retreat rate between ATM and InSAR may therefore merely reflect interannual changes in surface melt.

L. Bistrup Brae is a large glacier which flows northwards, opposite to Storstrømmen, until the two glaciers merge at the grounding line. It was named by Henning Bistrup as L. Bistrupsbrae during the 1906-08 Denmark expedition for his

father Lauritz Hans Christian Bistrup. L. Bistrup Brae is slow moving. Both ATM and InSAR indicate thickening at the grounding line. This glacier could also be a surge-type glacier in a quiescent phase.

5. Discussion

5.1. Mass Balance

The 11 glaciers listed in Table 3 have a total discharge of 62 km^3 ice yr^{-1} compared to a balance flux of 60 km^3 ice yr^{-1}, which means that the northern sector of the Greenland ice sheet is approximately in balance. The mass budget is similarly close to zero at the grounding line (Table 4). Numerous glaciers, however, exhibit positive or negative mass balance anomalies. Positive anomalies are typically associated with documented or suspected surging behavior. Some negative anomalies result from uncertainties in drainage boundaries between neighboring glaciers. If we included more realistic estimates of ice discharge from surge-type glaciers, positive anomalies would be reduced, yet the total mass budget would not change significantly.

The three largest glaciers, Petermann Gletscher, Nioghalvfjerdsbrae, and Zachariae Isstrøm, control 90% of the ice discharge listed in Tables 3-4. Their mass budget is -10±8% of the balance discharge at the ISR flux gate and is -11±8% at the grounding line. The mass budget of the larger glaciers is therefore almost certainly negative.

If we ignore the mass budget from the smaller and surge-type glaciers, the northern sector of the ice sheet appears to be loosing mass at a rate of 4±3 km^3 ice yr^{-1}. This rate of mass loss contributes 0.01 mm yr^{-1} global sea level rise [Jacobs et al., 1996], which is very small. Similarly, it contributes negligible ice sheet thinning if spread uniformly over the entire drainage area. Yet it could produce meter-scale glacier thinning if concentrated near the coast, for example over a 50-km-wide region upstream of the grounding line. The results of Krabill et al. [1999] indeed reveal negligible mass imbalance of the ice sheet interior but thinning near the coast, along the channels occupied by glaciers.

5.2. Coastal Thinning

The detection of grounding line migration with InSAR revealed that all glaciers developing a floating ice tongue exhibited grounding line retreat between 1992 and 1996, except slow moving L. Bistrup Brae and advancing Steensby Gletscher. The retreat rate varies from several hundred m yr^{-1} up to 1 km yr^{-1} and converts into ice thinning of 1 to 2 m yr^{-1}.

The magnitude of ice thinning inferred from the grounding line retreat is large compared to surface ablation (typically < 1 m ice yr^{-1} at the grounding line of northern glaciers [Thomsen et al., 1997]). The glacier retreat is therefore unlikely to be explained by enhanced surface melt between 1992 and 1996 from either warmer air temperatures or a longer melt season. Glacier thinning must therefore also be of dynamic origin.

Glacier ice may thin from enhanced longitudinal stretching, for example if the glacier velocity increases over time and space. In the case of the three largest glaciers discussed in section 4, an ice thinning of 1.5 m yr^{-1} would result from a longitudinal stretching of the ice by 0.0025 yr^{-1} if the grounding line ice thickness is 600 m. Over a distance of one glacier width (20 km), this represents a 50 m ice yr^{-1} increase in ice velocity, which is only 4% of the ice velocity at the grounding line. Measuring such a flow acceleration, or possibly lower acceleration if enhanced surface melt also contributes to glacier thinning, should be investigated in the future. An increase in coastal velocity of the outlet glaciers compared to the inland ice would cause coastal

thinning and grounding line retreat, while maintaining the ice sheet interior close to a state of mass balance.

If the thinning rates inferred from InSAR had prevailed over 1 century, the ice tongues of northern Greenland would not have survived, and we should have witnessed a major retreat of the glacier fronts. Petermann Gletscher, for one, did not experience a major retreat, although earlier reports suggested a much rougher surface for its ice tongue than at present [Koch, 1928]. Retreat of glacier floating tongues and sea ice has been more obvious in the northeast [Weidick, 1995]. One possibility, given the historical evidence for glacier front retreat, is that ice thinning and glacial retreat have accelerated in the last few decades.

5.3. Basal Melting

The study reveals the magnitude and extent of basal melting on northern Greenland floating ice tongues. Basal melt rates underneath the Ross and Filchner-Ronne ice shelves average a few tens of centimers of ice per year [Jacobs et al., 1996]. In northern Greenland the average melt rates are 10 times larger. Not only is basal melting high, but it is also the dominant form of mass ablation. Basal melting averages 5-8 m ice yr^{-1} on the floating tongues. In the proximity of the grounding line the rates are 3 times larger (Table 5). A higher melt rate is expected in these regions, because the ice draft reaches greater depths, and melting is facilitated at greater depths because of the pressure dependence of the ice melting point [Jenkins and Doake, 1991].

Near the grounding line, basal melting will influence ice flow in three ways. If basal melting is too large to maintain the ice in a state of mass balance, steeper surface gradients will be generated at the grounding line, which will increase the driving stress. Higher deviatoric stress gradients across the grounding line will also contribute to softening of the ice [Huybrecht, 1990]. Finally, the buttressing floating tongues will offer less resistance to inland outflow as they thin, which may increase ice discharge. High basal melting could therefore rapidly melt the floating tongues and perhaps cause rapid discharge of inland ice.

The influence of basal melting on ice sheet evolution has only been investigated for the Antarctic ice sheet, generally for modest levels of basal melting [Huybrecht and de Wolde, 1999]. The values of basal melting recorded here, in the proximity of grounding lines, are 2-5 times larger than in those simulations. Also, model simulations indicated clearly that changing the ocean conditions underneath the floating tongues is a far more efficient way to collapse ice shelves than increasing surface melt due to warmer air temperatures. Here, a 10% increase in basal melting near the grounding line of the glaciers would have drastic consequences on the sustainability of floating ice tongues: The floating sector of Petermann Gletscher would disappear completely in < 30 years. In contrast, a 10% increase in surface melt, from warmer or longer summers, is unlikely to disintegrate the floating tongues.

6. Conclusions

The advents of InSAR and other new technologies have permitted a major improvement in our knowledge of ice dynamics and mass balance of northern Greenland glaciers. From these data we have established a modern estimate of the mass budget of these glaciers, which is close to balance, except in the case of the three larger glaciers for which the mass budget is almost certainly negative. The detection of a systematic grounding line retreat of the glaciers provides strong evidence for their slow retreat and thinning along the coast, independent of their mass input and output. Furthermore, the glacier thinning rates inferred from the 1992-1996 grounding line retreat are

large. They cannot be explained by a few warm or longer summers, which suggests that ice thinning is of dynamic origin. Coincidentally, evidence for coastal dynamic thinning is more pronounced in other parts of Greenland [*Thomas et al.*, 2000].

Numerous surge-type glaciers are present in northern Greenland, despite its dry, cold climate. These glaciers contribute less than 10% of the total ice discharge. The resulting positive mass balance anomalies, however, emphasize the importance of gathering information on ice dynamics in order to interpret the results from radar and laser altimeters. Similarly, the interpretation of negative mass balance anomalies requires information on temporal and spatial changes in ice velocity.

InSAR has allowed a systematic assessment of basal melting on the northern floating tongues. The result is that the inferred melt rates exceed those recorded on large Antarctic ice shelves by 1 order of magnitude. It is clear neither how such high basal melting rates can be sustained over time by the surrounding ocean waters, nor how the floating tongues can or cannot survive in such an environment. In situ, timely observations of ocean conditions beneath the floating tongues are needed to confirm and better understand the remote sensing results.

References

Abdalati, W., W. Krabill, E. Frederick, S.Manizade, C. Martin, J. Sonntag, R. Swift, R. Thomas, W. Wright, and J. Yungel, Outlet glacier and margin elevation changes: Near-coastal thinning of the Greenland ice sheet, *J. Geophys. Res.*, this issue.

Bales, R., J. McConnell, E. Mosley-Thompson, and G. Lamorey. 2001. Accumulation map for the Greenland ice sheet: 1971-1990, *Geophys. Res. Lett.*, 28(15), 2967-2970, 2001.

Bamber, J., S. Ekholm, and W. Krabill, A new, high-resolution digital elevation model of Greenland fully validated with airborne laser altimeter data, *J. Geophys. Res.*, 106(B4), 6733-6745, 2001.

Braithwaite, R., Degree-day factor, energy balance, and the increased melting of the Greenland Ice Sheet under a warmer climate, *Rapp. Grønl. Geol. Unders.*, 155, 79-83, 1992.

Braithwaite, R., Positive degree-day factors for ablation on the Greenland ice sheet studied by energy-balance modelling, *J. Glaciol.*, 41(137), 153-160, 1995.

Braithwaite, R., Models of ice-atmosphere interactions for the Greenland ice sheet, *Ann. Glaciol.*, 23, 149-153, 1996.

Braithwaite, R., T. Konzelmann, C. Marty, and O. Olesen, Reconnaissance study of glacier energy balance in North Greenland, 1993-1994, *J. Glaciol.*, 44(147), 239-247, 1998.

Bøggild, C., N. Reeh, and H. Oerter, Modelling ablation and mass balance sensitivity to climate change of Storstrømmen, northeast Greenland, *Global Planet. Change*, 9, 79-90, 1994.

Chuah, T., S. Gogineni, C. Allen, and B. Wohletz, Radar thickness measurements over the northern part of the Greenland Ice Sheet, *Radar Syst. and Remote Sens. Lab. Tech. Rep. 10470-3*, Univ. of Kansas, Lawrence, 1996.

Davies, W., and D. Krinsley. The recent regimen of the ice cap margin in North Greenland, in *Symposium of Bergurgl, Austria*, (10-18 September 1962), *Int. Assoc. Sci. Hydrol., Pub. 58*, 119-130, 1962.

Ekholm, S., A full coverage, high-resolution, topographic model of Greenland computed from a variety of digital elevation data, *J. Geophys. Res.*, 101 (B10), 21,961–21,972, 1996.

Friedmann, A.., J. Moore, T. Thorsteinsson, J. Kipfstuhl, and H. Fischer, A 1200 year record of accumulation from northern Greenland, *Ann. Glaciol.*, 21, 19-25, 1995.

Goldthwait, R., Restudy of Red Rock ice cliff, Nunatarssuaq, Greenland,Tech. Rep. 224, 27 pp., U.S. Army Cold Reg. Res. and Eng. Lab., *Tech. Rep. 224*, 27 pp., Hanover, N.H., 1971.

Higgins, A., Glacier velocities from aerial photographs in north and

north-east Greenland, *Rapp. Grønl. Geol. Unders.*, 140, 102-105, 1988.

Higgins, A., North Greenland glacier velocities and calf ice production, *Polarforschung*, 60(1), 1-23, 1991.

Higgins, A., and A. Weidick, The world's northernmost surging glacier, *Z. Gletscherk. Glazialgeol.*, 24(2), 42-47, 1988.

Høy, T., Surveying and mapping in southern Peary Land, North Greenland, *Medd. Grønl.*, 182(3), 1-50, 1970.

Huybrecht, P., A 3-D model for the Antarctic ice sheet: A sensitivity study on the glacial-interglacial contrast, *Clim. Dyn.*, 5, 79-92, 1990.

Huybrecht, P., and J. de Wolde, The dynamic response of the Greenland and Antarctic ice sheets to multiple-century climatic warming, *J. Clim.*, 12(8), 2169-2188, 1999.

Jacobs, S., H. Helmer, and A. Jenkins, Antarctic ice sheet melting in the southeast pacific, *Geophys. Res. Lett.*, 23(9), 957-960, 1996.

Jenkins, A., and C. Doake, Ice-ocean interaction on Ronne Ice Shelf, Antarctica, *J. Geophys. Res.*, 96(C1), 791-813, 1991.

Joughin, I., D. Winebrenner, and M. Fahnestock, Observations of ice-sheet motion in Greenland using satellite radar interferometry, *Geophys. Res. Lett.*, 22(5), 571-574, 1995.

Joughin, I., S. Tulaczyk, M. Fahnestock, and R. Kwok, A mini-surge on the Ryder glacier, Greenland, observed by satellite radar interferometry, *Science*, 274(5285), 228-230, 1996.

Joughin, I., R. Kwok, and M. Fahnestock, Interferometric estimation of three-dimensional ice-flow using ascending and descending passes, *IEEE Trans. Geosc. Remote Sens.*, 36(1), 25-37, 1998.

Joughin, I., M. Fahnestock, R. Kwok, S. Gogineni, and C. Allen, Ice flow of Humboldt, Petermann and Ryder Gletscher, northern Greenland, *J. Glaciol.*, 45(150), 231-241, 1999.

Joughin, I., M. Fahnestock, D. McAyeal, J. Bamber, and S. Gogineni, Observation and analysis of ice flow in the largest Greenland ice stream, *J. Geophys. Res.*, this issue.

Koch, L., Contributions to the glaciology of north Greenland, *Medd. Grønl.*, 65(2), 181-464, 1928.

Kollmeyer, R., West Greenland outlet glaciers: An inventory of the major iceberg producers, in *World Glacier Inventory, Proceedings of the Workshop at Riederalp, Switzerland, 17-22 September 1978, Pub. 126*, p. 57-65, Int. Assoc. of Hydrol. Sci., Gentbrugge, Belgium, 1980.

Konzelmann, T., and R. Braithwaite, Variations of ablation, albedo and energy balance at the margin of the Greenland Ice Sheet, Kronprins Christian Land, eastern North Greenland, *J. Glaciol.*, 41(137), 174-182, 1995.

Krabill, W., E. Frederick, S. Manizade, C. Martin, J. Sonntag, R. Swift, R. Thomas, W. Wright, and J. Yungel, Rapid thinning of the southern Greenland ice sheet, *Science*, 283(5407), 1522-1524, 1999.

Le Provost, C., F. Lyard, J. Molines, M. Genco, and F. Rabilloud, A Hydrodynamic Ocean Tide Model Improved by assimilating a satellite altimeter-derived data set, *J. Geophys. Res.*, 103(C3), 5513-5529, 1998.

Lister, H., edited by R. A. Hamilton, Glaciology, 1, The balance sheet or mass balance, in *Venture to the Arctic*, pp. 167-188, Penguin Putman, New York, 1958.

Mock, S., Fluctuations of the terminus of Harald Moltke Brae, Greenland, *J. Glaciol.*, 6(45), 369-373, 1966.

Mohr, J., N. Reeh, and S. Madsen, Three-dimensional glacial flow and surface elevation measured with radar interferometry, *Nature*, 391, 273-276, 1998.

Nobles, L., Glaciological investigations, Nunatarssuaq ice ramp, north-western Greenland, U.S. Army Snow, Ice and Permafrost Res. Estab., U.S. Army Cold Reg. Res. and Eng. Lab., *Tech. Rep. 66*, 57 pp., Hanover, N. H., 1960.

Ohmura, A., and N. Reeh, New precipitation and accumulation maps for Greenland, *J. Glaciol.*, 37(125), 140-148, 1991.

Reeh, N., Greenland ice sheet mass balance and sea-level change, in *Glaciers, Ice Sheets, and Sea-Level: Effects of a CO_2-Induced Climatic Change*, pp. 155-171, Washington, D.C., Nat. Acad., 1985.

Reeh, N., Parametrization of melt rate and surface temperature on the Greenland ice sheet, *Polarforschung*, 59(3), 1989, 113-128,1991.

Reeh, N., C. Bøggild, and H. Oerter, Surge of Storstrømmen, a large outlet glacier from the inland ice of north-east Greenland, *Rapp. Grønlands Geol. Unders.*, 162, 201-209, 1994.

Reeh, N., C. Mayer, H. Miller, H. Thomsen, and A. Weidick, Present and past climate control on fjord glaciations in Greenland: Implications for IRD-deposition in the sea, *Geophys. Res. Lett.*, 26(8), 1039-1042, 1999.

Rignot, E., Tidal flexure, ice velocities and ablation rates of Petermann Gletscher, Greenland, *J. Glaciol.*, 42(142), 476-485, 1996.

Rignot, E., Hinge-line migration of Petermann Gletscher, north

Greenland, detected using satellite radar interferometry, *J. Glaciol.*, *44*(148), 469-476, 1998a.

Rignot, E., Radar interferometry detection of hinge-line migration on Rutford Ice Stream and Carlson Inlet, Antarctica, *Ann. Glaciol.*, *27*, 25-32, 1998b.

Rignot, E., K. Jezek, and H. Sohn, Ice flow dynamics of the Greenland ice sheet from SAR Interferometry, *Geophys. Res. Lett.*, *22*(5), 575-578, 1995.

Rignot, E., S. Gogineni, W. Krabill, and S. Ekohlm, Ice discharge from north and northeast Greenland as observed from satellite radar interferometry, *Science*, *276*(5314), 934-937, 1997a.

Rignot, E., S. Gogineni, W. Krabill, and S. Ekohlm, Mass balance of north Greenland - Response, *Science*, 278(5336), 209-209, 1997b.

Rignot, E., G. Buscarlet, B. Csatho, S. Gogineni, W. Krabill, and M. Schmeltz, Mass balance of the northeast sector of the Greenland ice sheet: A remote sensing perspective, *J. Glaciol.*, *46*(153), 265-273, 2000.

Thomas, R., W. Abdalati, T. Akins, B. Csatho, E. Frederick, S. Gogineni, W. Krabill, S. Manizade, and E. Rignot, Substantial thinning of a major east Greenland outlet glacier, *Geophys. Res. Lett.*, *27*(9), 1291-1294, 2000.

Thomsen, H., N. Reeh, O. Olesen, C. Bøggild, W. Starzer, A. Weidick, and A. Higgins, The Nioghalvfjerdsfjorden glacier project, North-East Greenland: A study of ice sheet response to climatic change, *Geol. Greenl. Surv. Bull.*, *176*, 95-103, 1997.

van de Wal, R., Mass-balance modelling of the Greenland ice sheet: A comparison of an energy-balance and a degree-day model, *Ann. Glaciol.*, *23*, 36-45, 1996.

Weidick, A., Greenland, in *Satellite Image Atlas of Glaciers of the World*, U.S. Geol. Surv. Prof. Pap., *1386C*, C1-C105, 1995.

E. Rignot, Jet Propulsion Laboratory, Radar Science and Engineering, Pasadena, CA 91109-8099. (eric@adelie.jpl.nasa.gov)

S. Gogineni, Radar Systems and Remote Sensing Laboratory, The University of Kansas, Lawrence, KS.

I. Joughin, Radar Science and Engineering Jet Propulsion Laboratory, Pasadena, CA 91109.

W. Krabill, Laboratory for Hydrospheric Processes, NASA Goddard Space Flight Center Wallops Facility,k Wallops Island, VA.